Spin-split antibonding molecular ground state in manganese-doped quantum dot molecules

Fanyao Qu,[1,2,*] L. Villegas-Lelovsky,[1] and P. C. Morais[1,3]
[1]*Instituto de Física, Universidade de Brasilia, 70910-900, Brasilia-DF, Brazil*
[2]*International Center for Condensed Matter Physics, University of Brasilia, 70910-900, Brasilia-DF, Brazil*
[3]*Huazhong University of Science and Technology, School of Automation, Wuhan 430074, China*
(Received 26 January 2015; revised manuscript received 14 May 2015; published 29 September 2015)

Tunnel coupling between two dots in manganese-doped InAs/GaAs quantum dot molecules (QDMs), valence band mixing, and *p-d* exchange interaction between holes and localized *d* electrons give rise to a tunability of charge, spin, and molecular orbitals. The interplay among them determines the nature of the molecular ground state. Remarkably, unlike usual diatomic molecules in which the bonding (BD) state is always the ground state, we found that the molecular ground state in Mn-doped QDMs is of antibonding (AB) character. Furthermore, it is a spin-split state and can be switched into the spin-split BD type. We also demonstrate that this unusual behavior can be tuned by the lateral confinement strength of the QDMs, the concentration, and the distribution of manganese as well as the electric field applied along the direction of the QDM axis.

DOI: 10.1103/PhysRevB.92.115445 PACS number(s): 71.70.Ej, 61.72.uj, 73.22.−f, 71.70.Gm

I. INTRODUCTION

It is known from quantum mechanics that when two identical atoms are brought together, each electron level splits into two levels, corresponding to bonding (BD) and antibonding (AB) molecular orbitals (MOs). The ground state of a diatomic molecule is the symmetric BD orbital, whereas the first excited state is the antisymmetric one. Similar molecular orbitals and energy order have also been found in artificial quantum dot molecules (QDMs) formed by double quantum dots with a thin barrier [1–6]. As the barrier thickness increases, however, an unusual behavior emerges: the molecular ground state changes its character from BD to AB. This anomalous energy order had been firstly predicted by multiband $k \cdot p$ theory in InAs QDMs [7] and then confirmed by magnetophotoluminescence spectroscopy [8,9]. A similar phenomenon has also been encountered in Ge/Si and in GaAs/AlGaAs QDMs [10]. The origin and the conditions for BD and AB crossings in undoped QDMs are understood as follows [11]. In single-semiconductor quantum dots (QDs), heavy holes (*hhs*) and light holes (*lhs*) are well separated due to quantum confinement, the ground state being characterized by the *hh* state. However, the mixture of *hh* with *lh* becomes relevant in the QDMs [12–14]. The simplest description of holes accounting for this mixing is the four-band Luttinger-Kohn (LK) Hamiltonian. Within this model, the tunneling rate of the hole is dominated by the *hh* character when the QDs are closely spaced. Nevertheless, as the barrier thickness increases, *hh* tunneling becomes small, but an additional correction induced by the *hh*-*lh* coupling emerges [12–14]. Because the correction and *hh* tunneling make opposite contributions to the energy of the hole ground state, the interplay between them might turn the molecular ground state to be an AB type. It is worth to point out that besides changing the barrier thickness there are other methods that can be utilized to tune the mixing of the heavy-light hole states, such as in-plane anisotropy of the quantum dot, an in-plane magnetic field, an electric field, etc.

QDs doped with a single magnetic ion or many magnetic ions is an emerging field of research and technology [15–42]. The former is a promising solotronic system because it accommodates both a charge and a single magnetic ion spin, which can be prepared and manipulated both electrically and optically through injection of spin-polarized carriers [19–21,38–42]. The latter provides important advantages for applications in magnetic memory and spintronic devices because it combines some of the properties of high-quality semiconductor crystals with magnetic properties of impurities [26–38]. Since the spin properties determined by the *p-d* exchange interaction depend strongly on the wave function of the hole at the magnetic ion, the switching of the nature of the ground state of QDMs results in a change of spin states. Therefore studying the dependence of the QDM ground-state characteristic on geometrical and physical parameters such as lateral confinement, barrier thickness, magnetic ion concentration, and an applied electric field opens up the possibility to tune both the molecular bond and spin-related property of the molecular ground state at will. It is not only useful for the development of applications in different fields, such as quantum information technology, quantum optics, spintronics, or light harvesting, but it has also unveiled new physics that had never been observed in natural molecules and conventional undoped QDs.

The manuscript is organized as follows. In Sec. II, we present our theoretical formulation in a didactic manner, starting from the single-Mn-doped bulk semiconductor, then moving to the multiband $k \cdot p$ theory for undoped, single-Mn-doped, and many-Mn-doped QDMs. In Sec. III, we discuss our results, starting from single-Mn-doped QDMs, then we move to the effects of an electric field in single-Mn-doped QDMs and we end with many-Mn-doped QDMs. We conclude our work in Sec. IV.

II. THEORETICAL FORMULATION

A. *p-d* exchange interaction energy in single-Mn-doped III-V semiconductors

The manganese atom has an atomic configuration of $[\mathrm{Ar}]3d^5 4s^2$. When introduced into a III-V semiconductor

*Corresponding author: fanyao@unb.br

like GaAs, the Mn will most likely substitute the Ga in the lattice [23]. At the Ga site in GaAs, the two 4*s* orbitals change to sp^3 orbitals to participate in the diamondlike bonds. Since the Mn has only two electrons in the 4*s* orbital and the As atom contributes five electrons to these bonds, one electron is missing. Hence the electronic configuration of the Mn atom becomes $3d^5$ + hole [33]. Electrons from neighboring bonds can fill this hole, which causes a detaching of the hole from the impurity. Then, the missing of one positive charge in the Mn core results in a negative charge in the vicinity of the Mn atom relative to the background [34]. The hole has a fourfold degeneracy inherited from the top of the valence band spin-orbit interaction (SOI). If we neglect the split-off band, the total angular momentum of the valence band states is equal to 3/2 due to the strong SOI. For convenience, in the following, we treat the hole as a pseudospin $s = 3/2$ object coupled to the Mn spin $M = 5/2$ via *p-d* exchange interaction [23]. The Hamiltonian of Mn-hole complex in III-V semiconductors can be described by the Zener model,

$$H_b = -\frac{\hbar^2}{2m^*}\nabla^2 - J_{pd}\sum_I \mathbf{s}\cdot\mathbf{M}_I\delta(\mathbf{r}-\mathbf{R}_I), \tag{1}$$

where m^* is the hole effective mass, J_{pd} is the *p-d* exchange coupling constant, $\mathbf{r}$ is the hole position, $\mathbf{M}_I$ and $\mathbf{R}_I$ are the spin and the position of Ith Mn^{2+} ion, respectively. The first term in H_b is the hole kinetic energy. The second one is the *p-d* exchange interaction Hamiltonian in which we sum over all of individual exchange interactions between one bound hole and the Mn ion spins. In particular, in the single Mn-doped GaAs, the expectation value of the exchange interaction potential, which leads to the formation of a magnetic polaron reads

$$\mathcal{H}_{h\text{-Mn}} = -J_{pd}\mathbf{s}\cdot\mathbf{M}|\psi(\mathbf{R}_0)|^2, \tag{2}$$

where $\psi(\mathbf{R}_0)$ is the hole wave function at the position $\mathbf{R}_0$ of the Mn^{2+} ion. To compact notation we assume $J_{\text{eff}} = J_{pd}|\psi(\mathbf{R}_0)|^2$, which denominates the effective *p-d* exchange interaction strength proportional to the probability of the hole at the Mn position. Therefore the energy E_b of Mn-hole complex is given by $E_b = E_k - J_{\text{eff}}\mathbf{s}\cdot\mathbf{M}$, where E_k denotes the hole kinetic energy. The *p-d* exchange interaction couples the spin angular momentum states of the **M** and **s** to give pair states with total spin J with a range of total spin quantum numbers $J = 1$, 2, 3, and 4. Because of this *p-d* exchange coupling, their spins are correlated and they are not good quantum numbers. However, H_b, M^2, s^2, J^2, and J_z form a complete set of commuting operators. Hence the energy levels of polaron read $E_b = E_k + 25J_{\text{eff}}/4 - J(J+1)J_{\text{eff}}/2$. The first two terms in E_b shift the position of the energy levels from its unperturbed position, whereas the last term splits the unperturbed level into a set of sublevels characterized by different values of J with degeneracy of $2J+1$. The exchange splitting ΔE_{ex} between consecutive levels changes with J, according to the following relation, $\Delta E_{ex} = (J+1)J_{\text{eff}}$. It is noted that the ΔE_{ex} increases with increasing the value of J as $\Delta E_{ex} = 2\times$, $3\times$, and $4\times J_{\text{eff}}$, respectively. For an antiferromagnetic coupling, the J_{eff} is negative so that the $J = 1$ state is the ground state. Hence, as long as the magnetic polaron is not distorted by perturbations that couple different J manifolds and the temperature is low enough, it is a good approximation to think of it as being a composite object with total spin $J = 1$.

B. Multiband $k\cdot p$ approach for undoped InAs/GaAs QDMs

Considering the coupling between *hh* ($s = 3/2$, $s_z = \pm 3/2$) and *lh* ($s = 3/2$, $s_z = \pm 1/2$) subbands, where s and s_z denote the band-edge Bloch angular momentum and its $z-$component, the Hamiltonian of a valence band hole in the cylindrical coordinate system (ρ,φ,z) is described by

$$\mathcal{H}_h = \mathcal{H}_{\text{KL}} + V(\rho,z)I, \tag{3}$$

where I is a 4×4 identity matrix. The first term in the $\mathcal{H}_h$ is the well known 4×4 Luttinger-Kohn Hamiltonian describing the anisotropic kinetic energy of the hole in zinc-blende crystals. In the effective mass approximation, the kinetic energy of the hole is described on the basis of Bloch functions at the top of the valence band (Γ_8 point), $|+3/2\rangle$,$|+1/2\rangle$, $|-3/2\rangle$, $|-1/2\rangle$, by the 4×4 Kohn-Luttinger Hamiltonian. When spanned in the s_z spin component basis, the $\mathcal{H}_{\text{KL}}$ [36] has the form

$$\mathcal{H}_{\text{KL}} = \frac{\hbar^2}{m_0}\begin{pmatrix} \mathcal{D}_{hh} & \mathcal{A}_- & 0 & \mathcal{B}_- \\ \mathcal{A}_-^* & \mathcal{D}_{lh} & \mathcal{B}_- & 0 \\ 0 & \mathcal{B}_-^* & \mathcal{D}_{hh} & \mathcal{A}_+ \\ \mathcal{B}_-^* & 0 & \mathcal{A}_+^* & \mathcal{D}_{lh} \end{pmatrix}, \tag{4}$$

where

$$\begin{aligned} \mathcal{D}_{hh} &= -\left(\frac{\gamma_1+\gamma_2}{2}\right)\{\hat{k}_+,\hat{k}_-\} - \left(\frac{\gamma_1-2\gamma_2}{2}\right)\hat{k}_z^2, \\ \mathcal{D}_{lh} &= -\left(\frac{\gamma_1-\gamma_2}{2}\right)\{\hat{k}_+,\hat{k}_-\} - \left(\frac{\gamma_1+2\gamma_2}{2}\right)\hat{k}_z^2, \\ \mathcal{A}_\pm &= \mp\sqrt{3}\gamma_3\hat{k}_\pm\hat{k}_z, \\ \mathcal{B}_\pm &= -\frac{\sqrt{3}}{2}\frac{\gamma_2+\gamma_3}{2}\hat{k}_\pm^2, \end{aligned} \tag{5}$$

with $k_\pm = k_x \pm ik_y$, $\mathbf{k} = -i\nabla$, and $\{\hat{k}_+,\hat{k}_-\} = \hat{k}_+\hat{k}_- + \hat{k}_-\hat{k}_+$. Here, m_0 is the electron rest mass, ∇ is the gradient operator, γ_1, γ_2, and γ_3 are the Luttinger-Kohn parameters defining the anisotropic effective masses and the coupling strength for *hh* and *lh* states. The second term in the Hamiltonian $\mathcal{H}_h$ is the confining potential, which reads $V(\rho,z) = V_\parallel(\rho) + V_\perp(z)$ with $V_\parallel(\rho)$ and $V_\perp(z)$ being the in-plane and the vertical component, respectively. For simplification and without loss of generality, we limit our attention on the dots having cylindrical symmetry with radius ρ and width ℓ, separated by an interdot distance $\mathcal{L}$, as shown in Fig. 1. Then, the in-plane potential term is chosen as

$$V_\parallel(\rho) = \tfrac{1}{2}K\rho^2, \tag{6}$$

where K scales the strength of the harmonic potential defined by the harmonic oscillator characteristic frequency $\omega = \sqrt{K/m_\parallel^*}$, with $m_\parallel^*$ being the in-plane hole effective mass. The vertical confinement potential is described by

$$V_\perp(z) = \begin{cases} 0, & -\ell_1 - \mathcal{L}/2 \leqslant z \leqslant -\mathcal{L}/2 \\ 0, & \mathcal{L}/2 \leqslant z \leqslant \ell_2 + \mathcal{L}/2 \\ \Delta V, & \text{otherwise} \end{cases}, \tag{7}$$

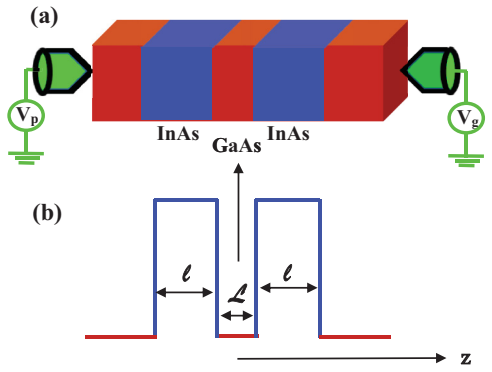

FIG. 1. (Color online) (a) Schematic diagram of an undoped quantum dot molecule created by in-plane gate voltages and vertical confinement. (b) Valence-band potential profile of InAs/GaAs quantum dot molecule. Here, ℓ, $\mathcal{L}$, V_g, and V_p denote dot size, GaAs barrier thickness, gate, and plunger voltage, respectively.

where $\triangle V$ is the band-offset of the materials at the interface between well and barrier. In our multiband expansion approach, the eigenfunctions of the Hamiltonian $\mathcal{H}_h$ are expanded by using an orthogonal set of functions

$$\Psi_v^h = \sum_{n,l,p,s_z} C_{n,l,p}^{s_z} f_{n,l}(\rho,\varphi) h_p(z)|s_z\rangle, \tag{8}$$

where $f_{n,l}(\rho,\varphi)$ and $h_p(z)$ are eigenfunctions of the following two single-band Schrödinger's equations:

$$\left(-\frac{\hbar^2}{2m_\parallel^*}\nabla_{\rho,\varphi}^2 + V_\parallel(\rho)\right) f_{n,l}(\rho,\varphi) = E_{n,l}^\parallel f_{n,l}(\rho,\varphi), \tag{9}$$

$$\left(-\frac{\hbar^2}{2m_\perp^*(z)}\frac{d^2}{dz^2} + V_\perp(z)\right) h_p(z) = E_p^\perp h_p(z), \tag{10}$$

where (n,l) denotes the quantum numbers of in-plane subbands, p denotes the z-direction index, and $m_\parallel^*$ and $m_\perp(z)^*$ are the anisotropic in-plane and in the z-direction hole effective masses. Then, the eigenvalues E_v^h and eigenfunctions $C_{n,l,p}^{s_z}(v)$ of $\mathcal{H}_h$ are obtained by the exact digitalization method.

Owing to the cylindrical symmetry of the confining potential, the total angular momentum operator, $\mathbf{F} = \mathbf{s} + \mathbf{L}$, commutes with the hole Hamiltonian, since the envelope functions have a definite angular momentum $\mathbf{L}$. Therefore $\mathbf{F}$ is a constant of motion and its eigenstates labeled by the good quantum number F_z will be also eigenfunctions of the Hamiltonian. For convenience, in our calculation, we replace the angular momentum of the envelope function L_z by F_z through the relation of $L_z = F_z - s_z$. Since the double quantum well solutions give rise to symmetric and antisymmetric states the Hilbert space of the hole wave functions $\Psi_{k,F_z}^h(\mathbf{r})$ can be split into two subspaces, labeled I and II, according to the combination of quantum numbers p and $F_z - s_z$. Hence the eigenvalue problem for the Hamiltonian in Eq. (3) can be solved independently for each class of states I and II, and for each value of F_z. Therefore the kth hole wave function (8) with parities I and II and total angular momentum z-projection F_z can be written as a four-component Luttinger spinor,

$$\Psi_{k,F_z}^{\mathrm{I(II)}} = \sum_{n,p} \begin{pmatrix} C_{n,F_z,2p-1(2p)}^{+\frac{3}{2},k} f_{n,F_z-\frac{3}{2}}(\rho,\varphi) h_{2p-1(2p)}(z)\left|+\frac{3}{2}\right\rangle \\ C_{n,F_z,2p(2p-1)}^{+\frac{1}{2},k} f_{n,F_z-\frac{1}{2}}(\rho,\varphi) h_{2p(2p-1)}(z)\left|+\frac{1}{2}\right\rangle \\ C_{n,F_z,2p(2p-1)}^{-\frac{3}{2},k} f_{n,F_z+\frac{3}{2}}(\rho,\varphi) h_{2p(2p-1)}(z)\left|-\frac{3}{2}\right\rangle \\ C_{n,F_z,2p-1(2p)}^{-\frac{3}{2},k} f_{n,F_z+\frac{1}{2}}(\rho,\varphi) h_{2p-1(2p)}(z)\left|-\frac{1}{2}\right\rangle \end{pmatrix}. \tag{11}$$

By substituting the expanded wave functions, Eq. (11), into $(\mathcal{H}_h - E_{k,F_z}^v)\Psi_{k,F_z}^v = 0$, here $v = \mathrm{I}$ or II, we obtain the matrix form of the Schrödinger equation. Then, the eigenvalues and eigenvectors of a valence band hole in the single QDM are computed by diagonalizing the matrix of the Hamiltonian $\mathcal{H}_h$. This variational procedure amounts to a progressive increase on the number of basis functions in order to achieve a convergence of low-energy eigenvalues of $\mathcal{H}_h$ with some desired accuracy. Since two states with opposite parities are orthogonal, the different hole eigenstates $|F_z| = 1/2, 3/2, 5/2, \ldots$ are doubly degenerate due to time-reversal symmetry and contain contributions from both hh and lh valence band states.

C. Multiband $k \cdot p$ theory for single-Mn-doped InAs/GaAs QDMs

After recalling the p-d exchange interaction in III-V semiconductors, let us focus our attention on it in the single-Mn-doped InAs/GaAs QDMs, as shown in Fig. 1. The system can be described by the following Hamiltonian, $\mathcal{H} = \mathcal{H}_h + \mathcal{H}_{h\text{-Mn}} + eFz$ [34]. The first term in $\mathcal{H}$ is the Hamiltonian of a valence band hole in the single QDM. The second term corresponds to the p-d exchange potential given by Eq. (2). The third one in $\mathcal{H}$ is the electrical potential energy induced by a uniform electric field F applied along the direction of the QDM axis. The eigenstate of the hole-Mn complex is obtained after expansion on the direct product between hole eigenstates $|\Psi_{\nu'}^h\rangle$ and the Mn-ion spin states $|M_z\rangle$ with z-projections $M_z = \pm 5/2, \pm 3/2$, and $\pm 1/2$, as

$$\Psi^{h\text{-Mn}}(\mathbf{r},\mathbf{R}_I) = \sum_{M_z}\sum_{\nu'} C_{\nu'}^{M_z}\left|\Psi_{\nu'}^h\right\rangle \otimes |M_z\rangle, \tag{12}$$

where ν' is a compact notation of the quantum numbers (k,F_z,ν) and the valence band hole wave function $\Psi_{\nu'}^h$ is provided by Eq. (11). Utilizing the expanded wave function of $\Psi^{h\text{-Mn}}(\mathbf{r},\mathbf{R}_I)$, the matrix of the Hamiltonian $\mathcal{H}$ is obtained. Then, the eigenvalues and eigenvectors of the polaron in the single QDM are computed by diagonalizing the matrix of the Hamiltonian $\mathcal{H}$. It is worth to arguing that the molecular orbitals of the QDMs formed by two identical QD potentials possess definite parities. For instance, the BD and AB states are even and odd functions, respectively. The molecular orbitals of the QDMs formed by two different QDs, however, will not exhibit the g and u symmetry properties of the former case. In general, they will be concentrated more around one nucleus than around the other. Nevertheless, some characteristics are preserved, such as BD MOs are less energetic than AB MOs and are in-phase of their atomic orbitals, whereas AB MOs are out-of-phase. Because the electric field F applied along the

QDM axis breaks the vertical mirror symmetry of the QDMs, the g and u symmetries are not preserved. Hence the molecular orbital is a mixture of the BD and AB states. Their weights in the ground state of the QDMs depend on the strength of electric field F. Similarly, the vertical mirror symmetry of the QDMs is also broken in the single-Mn-doped InAs/GaAs QDMs due to only one of the two dots containing Mn-ion. Thus the exchange field induces a hybridization of the BD and AB states too.

D. Multiband $k \cdot p$ theory for many-Mn-doped InAs/GaAs QDMs

The p-d exchange interaction Hamiltonian is composed of Ising and spin-flip parts. Their relative importance is determined by the degree of lh and hh mixing of the valence band states. For instance, in absence of lh-hh mixing, Mn-hole coupling becomes Ising-like. Otherwise, the Ising and spin-flip parts coexist, whereas the latter is approximately ten times smaller than the former [29]. Therefore, in many-Mn-doped diluted magnetic semiconductor InAs/GaAs QDMs, the p-d exchange interaction can be approximately described by an Ising-like model. Under this assumption, it is straightforward to write the matrix of $\mathcal{H}_{h\text{-Mn}}$ spanned in the Luttinger spinors, as

$$\mathcal{H}_{h\text{-Mn}} = -J_{pd} \sum_I s_z M_{z_I} \delta(\mathbf{r} - \mathbf{R}_I), \tag{13}$$

where s_z is the matrix form of the multiplet $s = 3/2$. After getting the exchange interaction Hamiltonian, the total Hamiltonian reads

$$\mathcal{H} = \mathcal{H}_h + \mathcal{H}_{h\text{-Mn}}. \tag{14}$$

Several approximations, such as the virtual-crystal approximation and mean-field theory, can be used to vastly simplify the above model. In the virtual-crystal approximation, the Mn^{2+} spins are replaced by a smooth spin density. Then $\mathcal{H}_{h\text{-Mn}}$ becomes

$$\mathcal{H}_{h\text{-Mn}} = -J_{pd} s_z \hat{M}_z(\mathbf{r}). \tag{15}$$

In homogeneous systems, $\hat{M}_z(\mathbf{r}) = N_0 x_{\text{Mn}} \hat{M}_{z-o}(\mathbf{r})$. In the mean-field approximation, quantum and thermal fluctuations of the local moment spin orientations are ignored. The hole spins only see averaged impurity spins and vice versa. Then, the local field experienced by the hole is given by $J_{pd} N_0 x_{\text{Mn}} \langle \hat{M}_{z-o}(\mathbf{r}) \rangle$. The eigenvalue problem can be solved by an expansion of the wave functions of a hole-Mn complex in the eigenstates of the Hamiltonian $\mathcal{H}_h$, as

$$\Phi = \sum_i A_i |i\rangle = \sum_{F_z,\nu,k} A_{F_z,\nu,k} \Psi^{\nu}_{k,F_z}, \tag{16}$$

where $|i\rangle$ denotes the ith eigenstate of the undoped QDMs system and i is a compact label for the set of quantum numbers F_z, k, and parity ν. Then, the averaged local magnetization of Mn ions in absence of an external magnetic field reads

$$\langle \hat{M}_{z-o}(\mathbf{r}) \rangle = \mu B_\mu \left(\mu \frac{J_{pd} \langle \hat{J}_z(\mathbf{r}) \rangle}{k_B T} \right), \tag{17}$$

where $B_\mu(x)$ is the Brillouin function, $\mu = 5/2$ and $J_{pd} \langle \hat{J}_z(\mathbf{r}) \rangle$ is the local mean field felt by the Mn, defined through the statistical mean value

$$\langle \hat{J}_z(\mathbf{r}) \rangle = \sum_{i,\sigma} f_{i\sigma} \langle \Psi_i | \hat{J}_z | \Psi_i \rangle_{\Omega_0}, \tag{18}$$

where Ω_0 is the unit cell volume and $f_{i\sigma} = e^{-E_{i\sigma}/k_B T} / \sum_j e^{-E_{j\sigma}/k_B T}$ is the probability occupancy of the state $|i,\sigma\rangle$. To clarify the contribution of each Bloch state, Eq. (18) is rewritten in the following form:

$$\langle \hat{J}_z(\mathbf{r}) \rangle = \langle \hat{J}_z^{hh\uparrow} \rangle + \langle \hat{J}_z^{hh\downarrow} \rangle + \langle \hat{J}_z^{lh\uparrow} \rangle + \langle \hat{J}_z^{lh\downarrow} \rangle. \tag{19}$$

The detailed calculation of $\langle J_z^\sigma(\mathbf{r}) \rangle$ can be found in Appendix B of Ref. [34]. After computing the statistical mean value of $\hat{J}_z(\mathbf{r})$, the mean-field ferromagnetic as well as the total Hamiltonians are obtained by

$$\mathcal{H}^{\text{MF}}_{h\text{-Mn}} = -J_{pd} N_0 x_{\text{Mn}} \langle \hat{J}_z(\mathbf{r}) \rangle \tag{20}$$

and

$$\mathcal{H}^{\text{MF}} = \mathcal{H}_h + \mathcal{H}^{\text{MF}}_{h\text{-Mn}}. \tag{21}$$

Since the p-d exchange interaction couples not only molecular orbitals with a different z-component F_z of total angular momentum but also the state with different parities, it is no longer possible to subdivide the full Hilbert space into two orthogonal subspaces, as it was done for the undoped case. Hence both the dimension and number of nonzero matrix elements of the total Hamiltonian matrix increase significantly. Notice that the $\langle \hat{J}_z(\mathbf{r}) \rangle$ is determined by the eigenvalues and eigenvectors of H^{MF}. In turn, the matrix elements of the H^{MF} depends on $\langle \hat{J}_z(\mathbf{r}) \rangle$. Hence this is a nonlinear problem. The solution of this magnetic polaron problem can only be obtained by self-consistently solving Eqs. (18) through (21). We start the self-consistent procedure from computing $\langle \hat{J}_z(\mathbf{r}) \rangle$. Then we construct the matrix of the exchange Hamiltonian $H^{\text{MF}}_{h\text{-Mn}}$. After that, we calculate all of the elements of the H^{MF} and diagonalize the matrix of the H^{MF} to obtain the eigenvalues and eigenstates. We repeat the above procedure until the required convergence is reached.

III. RESULTS AND DISCUSSION

A. Switch in nature of molecular ground state in undoped QDMs

A change in the nature of the conventional undoped QDM ground state from BD to AB by increasing the valence-band mixing has been reported in the literature [7–9]. This unusual behavior is reproduced by our calculation, as shown in Fig. 2 in which we plot the energy levels of the two lowest valence-band states of undoped QDMs as a function of interdot distance $\mathcal{L}$, obtained by means of a single-band model (a) and multiband $k \cdot p$ calculations (b). Both figures show that in a regime of large $\mathcal{L}$ the BD and AB are degenerate states, having the ground-state energy of an individual QD, as expected. As $\mathcal{L}$ decreases, the single-band model reckons on that each energy level of the isolated QDs splits into two molecular orbitals belonging to the pair, one lower and the other higher in energy as compared to the original atomic level. The lower energy orbital is BD, whereas the higher-energy orbital is AB. In

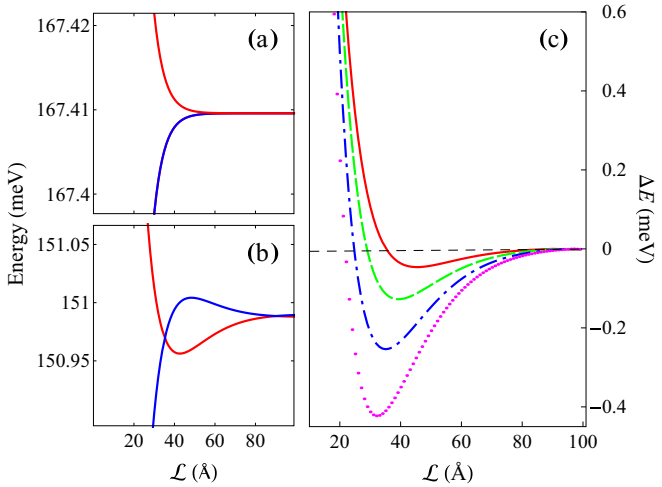

FIG. 2. (Color online) Energies of the two lowest heavy-hole bonding and antibonding states of pure (undoped) double QDs as a function of interdot distance ($\mathcal{L}$), for a dot size $\ell = 70$ Å and lateral confinement strength $\hbar\omega = 150$ meV, calculated by (a) single-band model and (b) multiband $k \cdot p$ formalism. (c) Energy differences between the BD (blue solid line) and AB (red solid line) states vs $\mathcal{L}$ for different confinement strengths $\hbar\omega = 150$ (solid red line), 200 (dashed green line), 250 (dash-dotted blue line), and 300 meV (magenta dotted line), computed by $k \cdot p$ approach.

contrast, the $k \cdot p$ theory predicts a crossover between BD and AB energy levels, indicating a change in character of the QDMs ground state. As is well known, in the single-band model calculation, both heavy-light hole coupling and SOI are neglected. In the multiband $k \cdot p$ approach, however, both contributions are included. Therefore the distinction between Figs. 2(a) and 2(b), i.e., BD-AB crossover, results from the heavy-light hole coupling and SOI. For a better insight of the mechanism of the AB-BD switch, Fig. 2(c) illustrates the energy difference between BD and AB states versus $\mathcal{L}$ under four different x-y plane confinement potentials $\hbar\omega$. Notice that, for small $\mathcal{L}$, the energy difference between AB and BD is positive, indicating that the ground state is BD. With increasing $\mathcal{L}$, however, BD-AB splitting decreases. At a critical value L_c the splitting becomes zero. After that, the energy difference turns to be negative, demonstrating a change in the character of the molecular ground state from BD to AB. Interestingly, this unusual behavior is strongly modulated by $\hbar\omega$. Although the BD-AB crossover takes place in all cases it occurs at shorter $\mathcal{L}$ as $\hbar\omega$ is increased. Meanwhile, the curve becomes deeper and deeper. The underlying physics can be understood as follows. The energy splitting between the BD and AB states depends on both interdot tunnel coupling and SOI. In absence of SOI, the tunneling rate is determined by the overlap between the hole orbitals of two individual dots, which decreases exponentially with increasing $\mathcal{L}$ at a rate dependent on the heavy-hole mass. When the SOI interaction is included, there is a correction to the tunneling coupling, arising from the small contribution of the light-hole component of the spinor. It therefore adds a small AB (BD) component to the BD (AB) state determined by the dominant heavy-hole component. The addition of this AB component increases the energy of the BD orbital (and vice versa for the AB orbital). For closely stacked two QDs, the SOI correction is small compared to the large tunnel coupling. Thus the splitting between BD and AB orbitals is mainly determined by tunnel coupling. While increasing the separation between two QDs the tunnel coupling becomes weaker. The correction induced by SOI, however, does not decrease as fast as the tunnel coupling term does, in part because of its light-hole origin. Then, one may expect that at certain $\mathcal{L}$, the SOI plays the same role as the tunnel coupling. As $\mathcal{L}$ is further increased, the SOI-correction term exceeds the tunnel coupling one. Then the AB state turns out to be the ground state of the QDMs. Furthermore, an enhancement of the quantum confinement of the individual QD weakens quantum tunnel coupling while enlarges SOI. Then the critical value of L_c at which the crossover between the energy levels of BD and AB orbitals occurs is reduced. The progressive deepening of the curves in Fig. 2(c) is also due to the systematic enhancement of the SOI, which scales with the in-plane confinement provided by $\hbar\omega$. Since the multiband $k \cdot p$ formulation, rather than the single-band model, provides a reliable physical behavior of the molecular ground state. It will be used from now on, except otherwise stated.

B. Spin-split AB molecular ground state in single-Mn-doped InAs/GaAs QDMs

The p-d exchange interaction strength J_{eff} depends strongly on the hole probability at the Mn^{2+}-ion location. Thus it can be modulated by changing the Mn-ion position. Except for the special case in which the manganese embedded exactly in the middle of the GaAs barrier in single-Mn-doped InAs/GaAs QDMs, the exchange interaction produces an asymmetric spin-dependent potential. Hence it breaks not only the mirror symmetry of the QDMs along the QDM axis, but also Kramer's degeneracy. Figures 3(b)–3(d) show the energies of the lowest molecular states in single-Mn-doped QDMs with manganese embedded in the upper (U) QD. For comparison purposes, the correspondent figure of undoped QDMs is shown in Fig. 3(a). One notices that a crossover between BD and AB states in undoped QDMs takes place as the dot-dot separation increases from 30 Å, as discussed in the previous section. In strong contrast, twelve branches that can be divided into two sets are observed in the single-Mn-doped QDMs. Among them, one is composed of six closely stacked levels (solid curves), the other (dotted curves) is constituted of well separated six branches. In addition, crossings take place among the states in the former set, whereas avoided crossings are found in the latter. In the regime of large $\mathcal{L}$, these twelve energy levels are gradually converging into seven branches. Among them, six possess equal interlevel distances in the latter set and the other one is located at the middle of them. Furthermore, with increasing exchange interaction, the six energy levels in the former set become much closer. Nevertheless, the interlevel distances are strongly enhanced by increasing J_{eff}. It is also worthwhile to notice that although the energy levels are split, an overall switch between BD and AB character of the ground molecular state is still observed. The underlying physics can be understood by virtue of the schematic diagram shown in Fig. 4. In the single-Mn-doped QDMs, only one of the two QDs is embedded with a Mn^{2+} ion. For clarity and without loss of generality, we suppose that the manganese is embedded

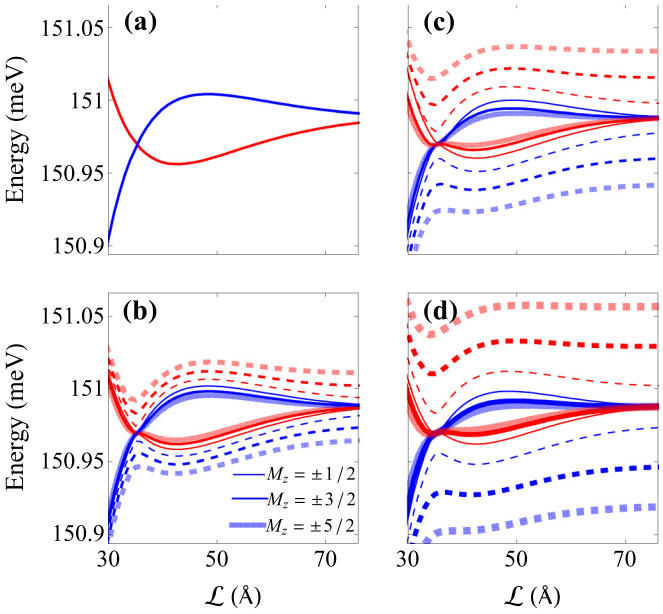

FIG. 3. (Color online) $\mathcal{L}$ dependence of the lowest lying BD and AB state energies of a heavy-hole in single-Mn-doped QDMs with a dot size $\ell = 70$ Å and lateral confinement strength $\hbar\omega = 150$ meV, for four effective exchange interaction values: (a) $J_{\text{eff}}/J_{pd} = 0.00$, (b) 0.01, (c) 0.02, and (d) 0.03. M_z is the z component of Mn spin.

in U-QD as shown in Fig. 4(a), sharing a common assumption about the Mn position with our calculations. It is also supposed that there is one orbital state in each of well separated QDs. Under these assumptions, one can safely expect that in the regime of large $\mathcal{L}$, there is only one energy level in the lower (L)QD, but there are six sublevels characterized by six components of Mn^{2+}-ion spin $M_z = \pm\frac{1}{2}, \pm\frac{3}{2}, \pm\frac{5}{2}$ in the U-QD. Since the tunneling coupling is vanishing small in the current

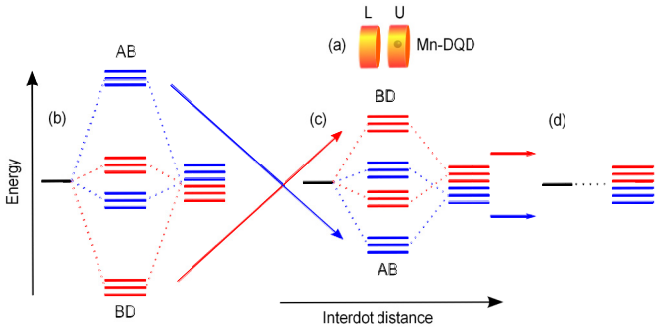

FIG. 4. (Color online) (a) Schematic view of a QDM doped with a single manganese represented by a sphere. L and U are abbreviations of lower and upper, respectively. (b)–(d) are schematic depictions of couplings between one atomic state of a hole in the undoped L-QD and six in the doped U-QD and the formation of molecular states for short, intermediate, and large interdot distances, respectively. In each panel, the left and right columns depict schematically the atomic energy levels of L- and U-QDs, where the middle column illustrates the molecular states. Dotted lines are guides to the eye that indicate the couplings. Red and blue arrows are also guides to the eye that show how the BD and AB states respond when $\mathcal{L}$ increases from the left to the right panels.

case, these six sublevels in the doped QD are symmetrically distributed around the energy level of the undoped QD, i.e., half above and half below the ground-state energy level of the L-QD, denominated by higher (red lines) and lower (blue lines) states, respectively, as illustrated in Fig. 4(d). As two QDs approach each other, the tunnel coupling is enhanced and molecular orbitals are created. The coupling between the state in L-QD and the six states in the U-QD results in the formation of six pairs of molecular orbitals. As is well known, a hybridization between two separate states raises the energy level of the lower energy state and lowers that of the higher energy state. Therefore these molecular orbitals belong to two groups. Among them group-I (II) arises from hybridizations of the state in L-QD with the higher (lower) states in U-QD, as shown in the middle of Fig. 4(c) by red (blue) lines. Because of weak tunnel coupling, the renormalization of atomic energy of individual QDs due to the hybridization is small. Therefore, in each group, there are two sets of three closely stacked levels, separated by the exchange interaction energy. In this regime, because of delocalization of the hole wave function, both heavy-light hole mixing and tunnel coupling exist. However, the valence band mixture is a predominant factor. Therefore the ground-state molecular orbital exhibits AB character. As $\mathcal{L}$ is further decreased, however, the tunnel coupling overcomes the valence band mixing and the molecular ground state is best characterized by BD type, as demonstrated in the middle of Fig. 4(b). Then, either crossover or anticrossing takes place for the molecular orbitals with the same or different z component of the total spin. Therefore a switch in the nature of the molecular ground state from the common BD to the AB type happens as the dot-dot separation increases.

C. Electrical field tuned AB molecular ground state in single-Mn-doped InAs/GaAs QDMs

In absence of electric field F, the molecular orbitals are orthogonal. Application of F along the QDM axis breaks its vertical mirror symmetry, shifting the energy levels of both dots overall and with respect to each other and causing a charge transfer between the two QDs. Then, the original zero-field orthogonal BD and AB states of QDMs are no longer decoupled. Instead, they become hybridized, which results in an avoided crossing and consequently the onset of an energy gap, as shown in Fig. 5 where the energies of the two lowest molecular states in a pure (undoped) QDM as a function of interdot distance are plotted. To reveal the characteristic of the molecular orbital, the weights of the BD (red curve) and AB (blue curve) components in the ground state of the QDM at $F = 0.04$ kV/cm are illustrated in the inset. Notice that the weight of the BD and AB components in the ground state is almost equal at $\mathcal{L} = 80$ Å . As $\mathcal{L}$ is decreased, the weight of AB increases, its counterpart decreases. Thus the molecular ground state is of the AB character. At $\mathcal{L} = 43$ Å, the former reaches its maximum and the latter drops to its minimum. After that, the BD starts to increase meanwhile the AB begins to decrease. When $\mathcal{L} = 36$ Å, the two components reach an equal weight again. While $\mathcal{L}$ is further decreased, the weight of BD type exceeds that of AB type. Consequently, the nature of the molecular ground state is characterized by BD type. It is also noted that the stronger the electric field the larger the band

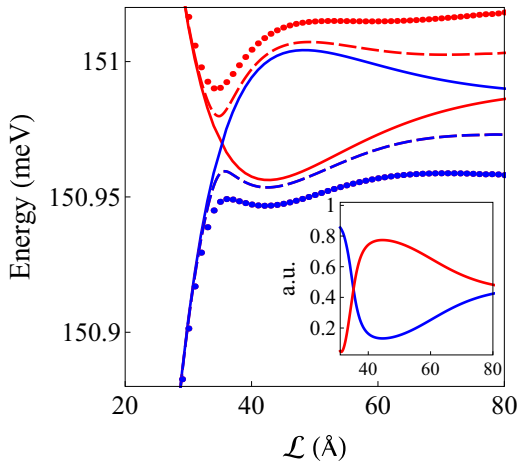

FIG. 5. (Color online) Energies of the two lowest molecular states in a pure (undoped) QDM with a dot size $\ell = 70$ Å and lateral confinement strength $\hbar\omega = 150$ meV, subjected to an electric field $F = 0$ (solid line), 0.02 (dashed line), and 0.04 kV/cm (dotted line). The inset shows the weights of the BD (red curve) and AB (blue curve) components of the ground state of the QDM at $F = 0.04$ kV/cm.

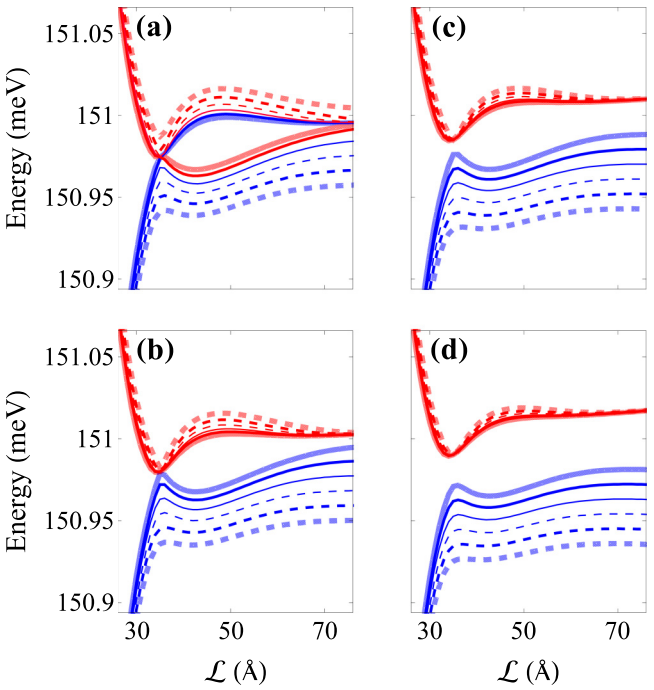

FIG. 6. (Color online) Energies of the lowest twelve states of the hole-Mn complex in a single-Mn-doped QDMs with a dot size $\ell = 70$ Å, lateral confinement strength $\hbar\omega = 150$ meV, and Mn^{2+} ion located at $z = \ell/2 + \mathcal{L}/2$, subjected to an electric field $F = 0.01$ (a), 0.02 (b), 0.03 (c), and 0.04 kV/cm (d). $J_{\text{eff}}/J_{pd} = 1\%$ is assumed in the calculation.

gap due to enhanced quantum confined Stark effect (QCSE). Furthermore, the QCSE depends strongly on $\mathcal{L}$. For a certain F, the QDMs with small $\mathcal{L}$ exhibit a weaker electric field effect than those with large $\mathcal{L}$. Then the energy levels are very close to their original zero-field counterparts. While increasing $\mathcal{L}$, however, the effects of the electric field become progressively stronger. In the regime of large $\mathcal{L}$, the tunnel coupling becomes vanishing and the energy levels of the two molecular states converge into two different values corresponding to the QCSE renormalized atomic energies of the U- and L-individual QDs. This strong F dependence allows us to tune the nature of the QD molecular orbitals electrically. Although F transforms a zero-field BD-AB crossing into an anticrossing, the main conclusion that is the switch of the character of the molecular ground state from BD to AB type still holds as $\mathcal{L}$ increases.

For the single-Mn-doped QDMs, both the p-d exchange interaction and applied electric field F break the vertical mirror symmetry of the system. The former induces the splitting of the molecular orbitals, whereas the latter induces an overall shift of the energy levels in both dots and a detuning between them, causing a charge transfer between QDs. Nevertheless, the p-d exchange interaction and F are not independent entities, but instead an interplay between them exists. Figure 6 shows the energies of the lowest twelve molecular spin orbitals as a function of the interdot distance for four different F values. In absence of F, there are two groups of molecular states: one (upper group) with a higher energy and the other (lower group) with a lower energy. In either group, three energy levels are closely stacked and others are well separated. However, the six twofold degenerated energy levels in the QDMs with large $\mathcal{L}$ are uniformly and symmetrically distributed around the energy level of the undoped QD. The electrical field F squeezes the energy levels belonging to the higher energy group, while spreads the energy levels in the other group, accompanied by opening up a gap. The stronger the F the bigger the gap and more closer the energy levels in the upper group. On the other hand, for a given F, the QCSE depends strongly on $\mathcal{L}$. In the regime of small dot-dot distance, tunnel coupling overcomes the effect of charge transfer. Then, molecular BD and AB are created and they extended to the whole system. Thus the overall twelve states arising from the exchange interaction between the hole and the Mn^{2+}-ion spin are observed. Increasing $\mathcal{L}$ leads to an enhanced Stark effect. Thus the ground-state hole is transferred from U to L dot. However, the hole lying in the first excited state is attracted to the U dot. Since the Mn^{2+} ion is embedded in the U dot, there is a vanishing exchange interaction in the ground state but a finite value in the first excited state. As a result, the six higher energy states are condensed by F, while the others are well separated by exchange interaction energy. Since F breaks down the mirror symmetry along the QDM axis, it induces coupling between the original independent zero field ($F = 0$) molecular orbitals, which leads to anticrossings as well as an opening of an energy gap. The larger the electric field the more pronounced the effects. It is worthwhile to comment that reversing the direction of F or changing the position of Mn^{2+} ion from the U to L dot, an inversion of energy spectra is expected.

To gain more insight into the spin and charge molecular physics, Fig. 7 depicts the energy spectra of the three lowest $|M_z| = 5/2$ states and the evolution of the correspondent orbitals of a hole-Mn complex in single-Mn-doped QDMs, subjected to an electric field $F = 2$ kV/cm. Notice that two of the three lowest states are coupled. As $\mathcal{L}$ increases, an

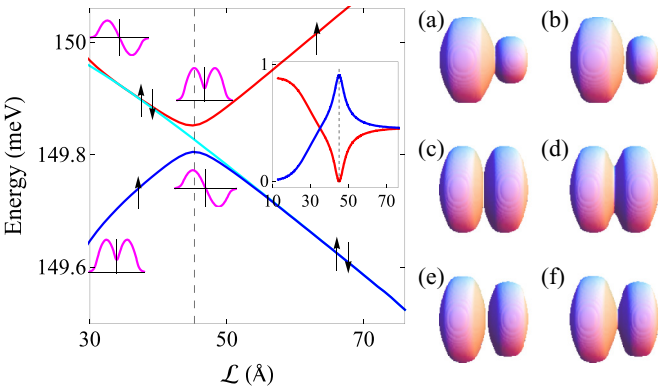

FIG. 7. (Color online) (Left) Energies of the three lowest $|M_z| = 5/2$ states of the hole-Mn complex in single-Mn-doped QDM with lateral confinement strength $\hbar\omega = 150$ meV and Mn^{2+} ion located at $z = \ell/2 + \mathcal{L}/2$, subjected to an electric field with a strength close to the resonance condition $F = 2$ kV/cm. The right-hand side inset plots the weight of the BD (blue line) and AB (red line) components in the ground state, whereas the middle and the left-hand side insets illustrate schematically the characteristics of the correspondent molecular orbital. Herein, the dashed lines are guides to the eye and indicate the critical point at which the switch in thecharacter of the ground state occurs. (Middle and right) Evolution of the correspondent molecular orbitals of the two coupled blue (middle) and red (right) $|M_z| = 5/2$ states as dot-dot separation $\mathcal{L}$ increases: [(a) and (b)] 35, [(c) and (d)] 45, and [(e) and (f)] 55 Å .

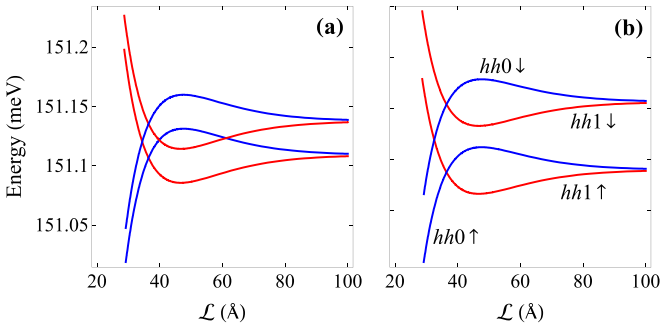

FIG. 8. (Color online) The first four lowest-lying $M_z = \pm 5/2$ molecular states of many-Mn-doped QDMs with the manganese concentration (a) $x_{Mn} = 0.020\%$ and (b) 0.025% (b) as a function of $\mathcal{L}$ for lateral confinement strength $\hbar\omega = 150$ meV.

anticrossing occurs, accompanied by a switch of the ground-state character from BD to AB. The character of the ground state is identified by the form of its orbital (right panel). At $\mathcal{L} = 30$ Å, the ground state is constituted by both BD and AB orbitals, but the BD component possesses a dominant weight. Hence an asymmetric orbital with a nonzero midway probability is observed, as shown in (a). As the two dots separate away, the weight of the AB component increases, while the BD component decreases. At $\mathcal{L} = 45$ Å, the orbital becomes almost symmetric with zero midway probability, as illustrated in (c). It indicates that the ground state is dominated by an antisymmetric AB orbital and the BD-component has only a vanishing contribution. Hence, the nature of the ground state has switched from the BD to AB character. As two dots are separated further, such as $\mathcal{L} = 55$ Å, the shape of the ground-state orbital changes slightly, but keeping the main feature unchanged. On the other hand, the right panel showing an evolution of molecular orbital of red curve provides a complementary information which gives an unambiguous support to our main conclusion. Finally, it is worthwhile to note that there is a state decoupled with both of above mentioned states. This decoupling is attributed to the different z component of total spin. It is important to mention that the exchange effect leads to an extra state shared by the BD and AB energy levels, thus providing a Mn- assisted tunneling resonance.

D. Effective Zeeman splitting of AB molecular ground state in many-Mn-doped InAs/GaAs QDMs

After understanding well the nature of single-Mn-doped QDMs ground state, we move our attention to diluted magnetic QDMs. In this case many manganese atoms are uniformly distributed in the system. The carrier mediated *p-d* exchange interaction induces an effective magnetic field which splits the atomic orbitals of individual QDs into spin-up and spin-down branches [34,37]. Since the tunnel coupling only hybridizes spinlike atomic orbitals, two pairs of the BD and AB states are formed. Among them, one is with an up-spin and the other with a down-spin, as shown in Fig. 8. The energy level separation between the two BD (blue lines) or AB (red lines) states are attributed to the effective Zeeman energy. As the concentration of manganese is increased from $x_{Mn} = 0.020\%$ to 0.025%, the two pairs are separated further due to the enhancement of the effective magnetic field.

IV. CONCLUSIONS

We present single- and multiband $k \cdot p$ calculations for both undoped and manganese-doped vertically stacked self-assembled InAs/GaAs QDMs. We found an unusual switch of the molecular ground state from BD to AB type as the dot-dot distance increases for both kinds of QDMs, which is unexpected in common diatomic molecules. In contrast to undoped QDMs, not only orbital-related but also spin-related new features are observed in Mn-doped QDMs. Furthermore, both of them can be tuned by either the concentration or the distribution of manganese, or the lateral confinement strength or the electric field applied along the direction of the QDM axis. For instance, in absence of electric field, there is only one pair of BD and AB states in undoped QDMs, there are six pairs in single-Mn-doped QDMs and two pairs in many Mn-doped QDMs. Furthermore, the six pairs of BD and AB states in single-Mn-doped QDMs are grouped into two sets. In one set, the energy levels are stacked together and the *p-d* exchange interaction tends to bring them closer. In the other group, however, the energy levels are well separated and taken farther apart by increasing the exchange interaction. Electric field remarkably tunes the gaps between anticrossing states.

ACKNOWLEDGMENT

Authors acknowledge financial support from the Brazilian agencies CNPq, FAPDF, and CAPES (FQ).

[1] H. J. Krenner, M. Sabathil, E. C. Clark, A. Kress, D. Schuh, M. Bichler, G. Abstreiter, and J. J. Finley, Phys. Rev. Lett. **94**, 057402 (2005).

[2] Stefan Folsch, Jesus Martinez-Blanco, Jianshu Yang, Kiyoshi Kanisawa, and Steven C. Erwin, Nat. Nanotechnol. **9**, 505 (2014).

[3] Alexander W. Holleitner, Robert H. Blick, Andreas K. Huttel, Karl Eberl, and Jorg P. Kotthaus, Science **297**, 70 (2002).

[4] T. Schmidt, R. J. Haug, K. von Klitzing *et al.*, Phys. Rev. Lett. **78**, 1544 (1997).

[5] M. Korkusinski and P. Hawrylak, Phys. Rev. B **63**, 195311 (2001).

[6] L. He, G. Bester, and A. Zunger, Phys. Rev. B **72**, 081311 (2005).

[7] G. Bester, A. Zunger, and J. Shumway, Phys. Rev. B **71**, 075325 (2005); W. Jaskólski, M. Zieliński, G. M. Bryant, and J. Aizpurua, *ibid.* **74**, 195339 (2006); J. I. Climente, M. Korkusinski, G. Goldoni, and P. Hawrylak, *ibid.* **78**, 115323 (2008).

[8] M. F. Doty, J. I. Climente, M. Korkusinski, M. Scheibner, A. S. Bracker, P. Hawrylak, and D. Gammon, Phys. Rev. Lett. **102**, 047401 (2009).

[9] J. I. Climente, Appl. Phys. Lett. **93**, 223109 (2008).

[10] A. I. Yakimov, A. A. Bloshkin, and A. V. Dvurechenskii, Semicond. Sci. Technol. **24**, 095002 (2009)

[11] M. F. Doty and J. I. Climente, *Quantum Dots: Optics, Electron Transport and Future Applications*, edited by Alexander Tartakovskii (Cambridge University Press, Cambridge, 2012).

[12] Y. H. Huo, B. J. Witek, S. Kumar, J. R. Cardenas, J. X. Zhang, N. Akopian, R. Singh, E. Zallo, R. Grifone, D. Kriegner, R. Trotta, F. Ding, J. Stangl, V. Zwiller, G. Bester, A. Rastelli, and O. G. Schmidt, Nat. Phys. **10**, 46 (2014).

[13] Mark L. Kerfoot, Alexander O. Govorov, Cyprian Czarnocki, Davis Lu, Youstina N. Gad, Allan S. Bracker, Daniel Gammon, and Michael Scheibner, Nat. Commun. **5**, 3299 (2014).

[14] W. J. Pasek, M. P. Nowak, and B. Szafran, Phys. Rev. B **89**, 245303 (2014).

[15] J. K. Furdyna, J. Appl. Phys. **64**, R29 (1988).

[16] H. Ohno, Science **281**, 951 (1998).

[17] T. Dietl, in *Handbook of Semiconductors*, edited by S. Mahajan (North Holland, Amsterdam, 1994).

[18] T. Jungwirth, J. Sinova, J. Masek, J. Kucera, and A. H. McDonald, Rev. Mod. Phys. **78**, 809 (2006).

[19] F. Qu and P. Hawrylak, Phys. Rev. Lett. **95**, 217206 (2005); **96**, 157201 (2006).

[20] Y. Léger, L. Besombes, J. Fernández-Rossier, L. Maingault, and H. Mariette, Phys. Rev. Lett. **97**, 107401 (2006).

[21] C. Le Gall, L. Besombes, H. Boukari, R. Kolodka, J. Cibert, and H. Mariette, Phys. Rev. Lett. **102**, 127402 (2009).

[22] Dale Kitchen, Anthony Richardella, Jian-Ming Tang, Michael E. Flatte, and Ali Yazdani, Nature (London), **442**, 436 (2006).

[23] A. M. Yakunin, A. Yu. Silov, P. M. Koenraad, J. H. Wolter, W. Van Roy, J. De Boeck, J.-M. Tang, and M. E. Flatte, Phys. Rev. Lett. **92**, 216806 (2004).

[24] J. K. Garleff, A. P. Wijnheijmer, A. Yu. Silov, J. van Bree, W. Van Roy, J.-M. Tang, M. E. Flatte, and P. M. Koenraad, Phys. Rev. B **82**, 035303 (2010).

[25] T. O. Strandberg, C. M. Canali, and A. H. MacDonald, Phys. Rev. Lett. **106**, 017202 (2011).

[26] D. H. Lee and J. A. Gupta, Science, **330**, 1807 (2010).

[27] J. I. Climente, M. Korkusiński, P. Hawrylak, and J. Planelles, Phys. Rev. B **71**, 125321 (2005).

[28] A. O. Govorov and A. V. Kalameitsev, Phys. Rev. B **71**, 035338 (2005); A. O. Govorov, *ibid.* **72**, 075359 (2005).

[29] J. Fernández-Rossier, Phys. Rev. B **73**, 045301 (2006).

[30] J. van Bree, P. M. Koenraad, and J. Fernández-Rossier, Phys. Rev. B **78**, 165414 (2008).

[31] Xiaojing Li and Kai Chang, Appl. Phys. Lett. **92**, 251114 (2008); **92**, 071116 (2008).

[32] Sucismita Chutia and A. K. Bhattacharjee, Phys. Rev. B **78**, 195311 (2008).

[33] J. Schneider, U. Kaufmann, W. Wilkening, M. Baeumler, and F. Köhl, Phys. Rev. Lett. **59**, 240 (1987).

[34] L. Villegas-Lelovsky, Fanyao Qu, L. O. Massa, V. Lopez-Richard, and G. E. Marques, Phys. Rev. B **84**, 075319 (2011).

[35] L. Villegas-Lelovsky, Fanyao Qu, V. Lopez-Richard, and G. E. Marques, Phys. Rev. B **82**, 193304 (2010).

[36] F. B. Pedersen and Y.-C. Chang, Phys. Rev. B **53**, 1507 (1996).

[37] C. Gould, A. Slobodskyy, D. Supp, T. Slobodskyy, P. Grabs, P. Hawrylak, F. Qu, G. Schmidt, and L. W. Molenkamp, Phys. Rev. Lett. **97**, 017202 (2006).

[38] J. Kobak, T. Smoleński, M. Goryca, M. Papaj, K. Gietka, A. Bogucki, M. Koperski, J.-G. Rousset, J. Suffczyński, E. Janik, M. Nawrocki, A. Golnik, P. Kossacki, and W. Pacuski, Nat. Comm. **5**, 3191 (2014).

[39] A. Kudelski, A. Lemaître, A. Miard, P. Voisin, T. C. M. Graham, R. J. Warburton, and O. Krebs, Phys. Rev. Lett. **99**, 247209 (2007).

[40] E. Baudin, E. Benjamin, A. Lemaître, and O. Krebs, Phys. Rev. Lett. **107**, 197402 (2011).

[41] M. Goryca, P. Plochocka, T. Kazimierczuk, P. Wojnar, G. Karczewski, J. A. Gaj, M. Potemski, and P. Kossacki, Phys. Rev. B **82**, 165323 (2010).

[42] D. Thuberg, D. E. Reiter, V. M. Axt, and T. Kuhn, Phys. Rev. B **88**, 085312 (2013).